American Journal of Pathology, Vol. 161, No. 5, November 2002

Constitutive Retinal CD200 Expression Regulates Resident Microglia and Activation State of Inflammatory Cells during Experimental Autoimmune Uveoretinitis

Cathryn Broderick,* Robert M. Hoek,† John V. Forrester,* Janet Liversidge,* Jonathon D. Sedgwick,‡ and Andrew D. Dick§

From the Department of Ophthalmology, University of Aberdeen, Aberdeen, United Kingdom; the Division of Ophthalmology,§ University of Bristol, Bristol, United Kingdom; the Department of Immunology,† University Medical Centre, Utrecht, The Netherlands; and DNAX Research Incorporated,‡ Palo Alto, California*

Recent evidence supports the notion that tissue OX2 (CD200) constitutively provides down-regulatory signals to myeloid-lineage cells via CD200-receptor (CD200R). Thus, mice lacking CD200 ($CD200^{-/-}$) show increased susceptibility to and accelerated onset of tissue-specific autoimmunity. In the retina there is extensive expression of CD200 on neurons and retinal vascular endothelium. We show here that retinal microglia in $CD200^{-/-}$ mice display normal morphology, but unlike microglia from wild-type $CD200^{+/+}$ mice are present in increased numbers and most significantly, express inducible nitric oxide synthase (NOS2), a macrophage activation marker. Onset and severity of uveitogenic peptide (1-20) of interphotoreceptor retinoid-binding protein-induced experimental autoimmune uveoretinitis is accelerated in $CD200^{-/-}$ mice and although tissue destruction appears no greater than seen in $CD200^{+/+}$ mice, there is continued increased ganglion and photoreceptor cell apoptosis. Myeloid cell infiltrate was increased in $CD200^{-/-}$ mice during experimental autoimmune uveoretinitis, although NOS2 expression was not heightened. The results indicate that the CD200:CD200R axis regulates retinal microglial activation. In $CD200^{-/-}$ mice the release of suppression of tonic macrophage activation, supported by increased NOS2 expression in the $CD200^{-/-}$ steady state accelerates disease onset but without any demonstration of increased target organ/tissue destruction. ***(Am J Pathol 2002, 161:1669–1677)***

It has long been recognized that resident macrophages isolated from different tissues and anatomical sites are heterogeneous and that resident macrophages are adapted to the local microenvironment.[1,2] Data obtained from developmental studies,[3] macrophage proliferation,[4] and depletion studies[5] indicate that macrophage development, differentiation, and proliferation are regulated by the tissue microenvironment.[6] Although many soluble factors such as M-CSF and GM-CSF and various cytokines[7,8] play a major role in this regulation and modification, to date, relatively few surface receptor factors have been identified for this role. Leukocyte function, including macrophages, may be regulated by the integration of both activation and inhibitory signals received through cell surface receptors.[9] In common with most of the inhibitory receptors is the conservation of immunoreceptor tyrosine-based inhibitory motifs[10] in the cytoplasmic domains, although inhibitory molecules such as CTLA-4 lack this motif.[11] Targeted disruption of such molecules leads to an increase in autoimmune disorders, which are frequently fatal.[11] A paradigm has emerged in which the strength of the opposing activating and inhibitory signals determine the initiation, amplification, and termination of immune responses.[12]

More recently, investigations of CD200 (OX2), a 41- to 47-kd member of the immunoglobulin superfamily and its receptor (CD200R), have indicated that macrophages and granulocytes are restrained from tissue-damaging activation through CD200R signaling. In all species so far tested, CD200 has a wide distribution and expression on neurons, activated T cells, B cells, follicular dendritic cells, and endothelium.[13–15] By contrast the CD200R is expressed predominantly by cells of the myeloid lineage[14,16] including microglia (MG)[14] inferring a significant role for the CD200/CD200R axis within the central nervous system. Structurally, CD200R resembles CD200, with two IgSF domains, but with a larger cytoplasmic domain, which suggests CD200R engagement may lead to intracellular signals affecting macrophage function.[16] Regulation of macrophage function is supported by the following observations in $CD200^{-/-}$ mice: significant in-

Supported from grants from the Iris Fund for the Prevention of Blindness, the Royal College of Surgeons of Edinburgh, and Schering-Plough Corporation (to DNAX).

Accepted for publication July 22, 2002.

Address reprint requests to Professor Andrew D. Dick. Division of Ophthalmology, Bristol Eye Hospital, Lower Maudlin St., Bristol, United Kingdom BS1 2LX. E-mail: a.dick@bristol.ac.uk.

crease in numbers of myeloid-derived cells within lymphoid organs,[15] accelerated onset of experimental autoimmune encephalomyelitis, and conversion of C57BL/6 mice from resistant to susceptible to collagen-induced arthritis.[15] Increased central nervous system (CNS) macrophage/MG responses were also observed, including aggregate formation in the spinal cord, an effect normally associated with inflammation or neurodegeneration.[15] Although it seems that CD200:CD200R engagement may modulate myeloid cell turnover as well as development of autoimmune disease, it is unclear from the reported experiments how this happens. In particular, it is unclear whether resident MG or perivascular macrophage activation in the CNS is the predominant event in predisposing $CD200^{-/-}$ mice to experimental autoimmune encephalomyelitis.

We therefore wished to assess whether loss of CD200:CD200R engagement within the retina (a neural tissue containing comparatively few MG) also results in increased tissue destruction during experimental autoimmune uveoretinitis (EAU). As in the brain and spinal cord, CD200 is expressed on the axons of glial fibrillary acidic protein-negative neurons, and on choroidal and retinal vascular endothelium within human, rat, and mouse retina and we have described this previously.[17] Murine EAU is a $CD4^+$ T-cell-mediated destruction of the neuroretina and photoreceptors of the eye.[18,19] EAU has the advantage of not only determining cellular infiltrate but the model also permits the semiquantitative documentation of the extent of tissue destruction.[18,20]

Materials and Methods

Animals and Induction of EAU

CD200-deficient mice ($CD200^{-/-}$) of background strain C57BL/6 were generated by DNAX, Palo Alto, CA[15] and breeding colonies established within the Biological Services Unit of Aberdeen University, and University of Bristol, UK, for further experimentation. All animals were specific pathogen-free, isolator-reared, and maintained in accordance to Home Office Regulations for Animal Experimentation, UK, and conformed to the Association for Research in Vision and Ophthalmology statement for the use of animals in Ophthalmic and Vision Research. C57BL/6 wild-type ($CD200^{+/+}$) mice were purchased from Harlan Olac, UK. All animals were immunized between 6 to 8 weeks of age. For each experiment, groups of 24 $CD200^{+/+}$ and 24 $CD200^{-/-}$ mice were immunized by a subcutaneous injection of 500 μg of peptide 1-20 interphotoreceptor retinoid-binding protein (IRBP) (Dr. Arthur Moir, University of Sheffield, Sheffield, UK) per mouse, emulsified in vol/vol complete Freund's adjuvant (2.5 mg/ml *Mycobacterium tuberculosis*). Mice were administered an additional intraperitoneal injection of 1.5 μg of *Bordetella* pertussis toxin. Mice were sacrificed by CO_2 asphyxiation at days 0, 10, 16, and 21 or 23 after immunization. At the specified time points, eyes were enucleated for histological grading, immunohistochemistry, and flow cytometric analysis and lymphoid tissue dissected (spleen, inguinal and iliac lymph nodes) to determine proliferative and cytokine responses.

Immunohistochemistry and Retinal Whole-Mount Immunofluorescence

Sex- and age-matched $CD200^{-/-}$ and $CD200^{+/+}$ mice were sacrificed by CO_2 asphyxiation. Eyes were dissected, and either snap-frozen in OCT and 6- to 8-μm cryostat sections prepared for immunocytochemistry (Leica, UK), or placed in neutral buffered formalin for paraffin embedding and hematoxylin and eosin staining for histological scoring. For grading, at least three sections from each eye were scored in a masked manner using a semiquantitative scoring system, which has been described[18] and combines the extent of the inflammatory infiltrate and tissue damage in the anterior and posterior chambers of the eye. All results are expressed as mean $\pm$ 1 SEM. Comparison of histological assessment of disease in $CD200^{-/-}$ and $CD200^{+/+}$ were analyzed using the unpaired *t*-test (Graphpad Instat Software), and *P* values equal to or less than 0.05 were considered significant.

For immunofluorescence, increased background staining because of endogenous avidin was prevented by preincubation with an avidin block (Vector Laboratories, Burlingame, CA) and 10% normal rabbit serum diluted in Tris-buffered saline. Primary monoclonal antibody (mAb) against F4/80, MOMA-1, MHC class II (all obtained from Serotec, UK), inducible nitric oxide synthase (NOS2) (clone 6, 1:100; Transduction Laboratories, UK), OX90 (anti-mouse CD200, 1:75, kindly supplied by G Wright, Oxford, UK) were used at previously determined optimized concentrations after dilution in biotin block (Vector kit). After a 1-hour incubation at room temperature slides were washed thoroughly in Tris-buffered saline. Primary antibodies were then detected with biotin-labeled rabbit anti-rat Ig (DAKO, Ely, UK), visualized using SA:ABC AP (DAKO) and fast red substrate, and lightly counterstained with hematoxylin. Apoptotic cells in the sections were detected using the diaminobenzidine- and fluorescein isothiocyanate (FITC)-labeled terminal dUTP nick-end labeling (TUNEL) method exactly according to the instructions of the kit manufacturer (Trevigen, AMS Biotechnological Ltd., UK, and Promega, Madison, WI). Retinal positive cells were counted in five fields in each of three sections per eye. Statistical significance was calculated using the unpaired *t*-test (Graphpad Instat Software).

For whole-mount assessment, eyes were enucleated and fixed in 1% paraformaldehyde for 1 hour. Biomicroscopic dissection of whole retina was achieved after removal of the cornea and extirpation of the lens and vitreous body. The retina was washed three times for 5 minutes in 1% bovine serum albumin/phosphate-buffered saline (BSA/PBS) and incubated at room temperature for 15 minutes in hyaluronidase (10 μg/ml, Sigma, Dorset, UK) to digest any remaining vitreous on the surface of the retina. Tissue was then washed three times for 10 minutes in 1%BSA/PBS and 0.2% saponin and subsequently in-

cubated for 1 hour at room temperature with unconjugated primary antibody-F4/80 (1:25, Serotec) diluted in 1%BSA/PBS and 0.2% saponin; each retina was individually placed in a 24-well culture plate. F4/80-positive cells were visualized by incubation with FITC-conjugated goat anti-rat IgG (1:100, Sigma, UK). Retina was finally mounted with great care to prevent folding using Vectashield (Vector Laboratories) and fluorescence was observed using appropriate filters using an Olympus BH2-RFC microscope.

Flow Cytometric Analysis

The phenotype of infiltrating and resident retinal leukocytes was investigated after isolation of cells at different phases of EAU. Retinas were dissected as above and single-cell suspensions prepared by passing through a 250-μm metal sieve. Cellular debris and nonviable cells were removed by a density gradient (Percoll; Amersham, UK) as previously described, which enriched for leukocytic populations.[20] Cell surface antigen expression was determined using mAb obtained from Pharmingen unless otherwise stated and included CD3, CD4, CD69, CD11b, CD45, MHC class II, CD86, CD40, F4/80 (Serotec, UK), MOMA-1 (Serotec, UK), and OX90 (G Wright, Oxford, UK) either unconjugated or conjugated to FITC, phycoerythrin, or biotin for subsequent two- and three-color analysis as previously described.[20] Intracellular staining for Ki67:FITC (Pharmingen, UK) required an additional permeabilizing step, protocol as suggested by the manufacturer. Biotin-labeled antibodies were detected by addition of SA:APC (1:400; Pharmingen, La Jolla, CA). OX90 (anti-mouse CD200) mAb was unconjugated and expression detected with goat anti-rat FITC (1:100; Serotec, UK). Staining was performed using fluorescence-activated cell sorting (FACS) buffer (PBS/BSA/10 mmol/L NaN_3) for washes. All reagents, buffers, and incubations were performed and kept at 4°C. Negative isotype controls and single positive controls were performed to allow accurate breakthrough compensation and background limits. Cells were incubated sequentially with primary mAb, anti-rat IgG (whole molecule) FITC conjugate in the presence of 5% normal mouse serum (NMS) if unconjugated, blocked with 10% normal mouse serum/normal rat serum (NMS/NRS), biotinylated second antibody with phycoerythrin-conjugated third antibody, and finally SA-APC for three-color analysis. Acquisition was performed using a FACS Calibur (Becton Dickinson) and analysis using Cellquest software. A total of 10,000 events were collected and gates and instrument settings were set according to forward and side scatter characteristics. Fluorescence analysis was performed after further back gating to exclude dead cells and background staining.

Proliferation Assay and Cytokine Analysis

Splenocyte responses were obtained from single-cell suspensions after mechanical dissociation of the tissue through a 250-μm metal sieve. The cells were resuspended at a final concentration of 2×10^6 cells/ml. One hundred μl of cells were then added to a 96-well plate, containing 100 μl of either complete RPMI (cRPMI; RPMI plus 5% fetal calf serum, 1% L-glutamine, 1% sodium pyruvate, 1% non-essential amino acids (NEAA), 0.5% mercaptoethanol, 2% penicillin/streptomycin, unstimulated control population), cRPMI containing Con A (2.5 μg/ml, positive response control), 1-20 IRBP peptide (5 μg/ml), or cRPMI containing whole IRBP (10 μg/ml), which was prepared as previously described.[21,22] Cells were incubated for 48 hours, at which time they were pulsed with 1 μl per well of ^{3}H-thymidine (Amersham, UK) and further incubated for 18 hours. Cells were harvested onto glass filter paper and counts per minute recorded as mean of triplicate wells. Stimulation index (mean stimulation of triplicate wells of stimulant divided by mean stimulation of triplicate wells of controls) was used to present proliferation data because analysis was performed on different days. Statistical analysis was performed using the unpaired *t*-test and $P < 0.05$ was considered significant.

At each time point, supernatants from splenocytes that were cultured (1×10^6/ml) for 48 hours, stimulated with either cRPMI or peptide (1-20 IRBP; 5 μg/ml) or IRBP (10 μg/ml) were removed and kept at −20°C until further analysis. Cellular interferon (IFN)-γ and interleukin (IL)-10 production was assessed using Quantikine ELISA (enzyme-linked immunosorbent assay) kits (R&D Systems, UK), following the manufacturer's instructions, with purified capture and biotinylated detector antibody pairs and standardized with recombinant cytokine to obtain a standard curve. The detection level of each kit was 2.0 pg/ml and 4.0 pg/ml, respectively. Results were presented as mean ± SD of triplicate wells of pooled samples of animals from each group and differences were considered significant if $P < 0.05$ using an unpaired *t*-test. In all cases, the nonstimulated cell supernatant cytokine levels were below detection.

Results

Retinal Microglia of CD200$^{-/-}$ Mice Are Activated (NOS2$^+$) and Are Increased in Numbers

In concurrence with previous results we again show that CD200 is expressed widely on retinal vascular endothelium and glial fibrillary acidic protein-negative neurons and during EAU (Figure 1A).[15–17] CD200 is expressed throughout the neuronal layers of the retina (N, Figure 1A) and endothelium (E, Figure 1A) of inner retinal vasculature, which has been previously verified by two-color immunohistochemistry.[17] As expected, concurrent immunodetection of CD200 on CD200$^{-/-}$ ocular tissue is negative (Figure 1B). The proportion of resident retinal CD45$^+$CD11b$^+$ cells (MG and perivascular macrophages) as determined by flow cytometric assessment of single cell suspension of retinal cell isolate, was increased significantly by 30% representing 1.7 ± 0.59% of retinal cells in CD200$^{-/-}$ compared to 1.3 ± 0.6% of retinal cells in CD200$^{+/+}$mice ($P = 0.04$, Mann-Whitney

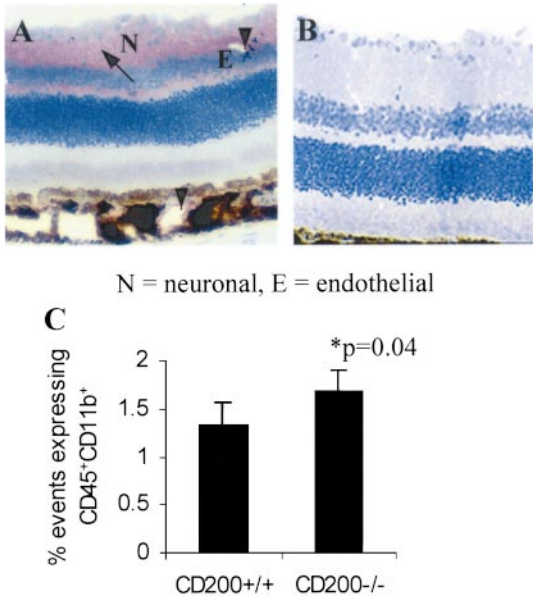

Figure 1. APAAP immunohistochemical detection of CD200 expression in retina of $CD200^{+/+}$ and $CD200^{-/-}$ mice. **A:** CD200 is abundantly expressed on endothelium (E) (**arrowhead**) and neuronal axons and cell bodies in $CD200^{+/+}$mouse (N) (**arrow**) normal retina but is expectedly absent in $CD200^{-/-}$ mice (**B**). **C:** MG (defined by $CD45^{+}CD11b^{+}$ population by two-color flow cytometric analysis) are present in significantly greater numbers within $CD200^{-/-}$ retina ($n = 7$, $P = 0.04$). Results shown are percentages of total events collected. Unlike CNS and rat retina,[23] mouse retinal MG and macrophages express equivalent levels of CD45, and cannot therefore be differentiated by $CD45^{low}$ or $CD45^{high}$, respectively. Original magnifications: ×250 (**A**); ×300 (**B**).

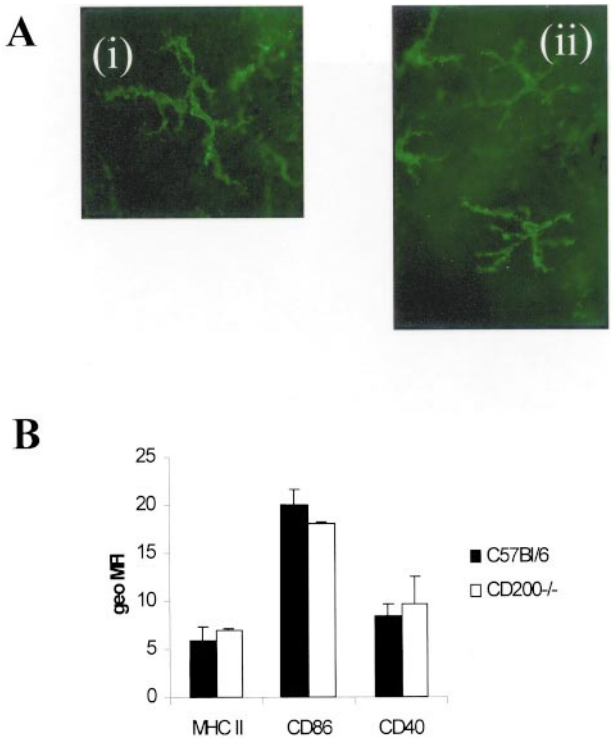

Figure 2. $CD200^{-/-}$ MG have normal morphology and express low amounts of MHC class II and co-accessory molecules. **A:** Retinal whole-mount immunofluorescence demonstrating F4/80 expression shows that the morphology of $CD200^{-/-}$ MG do not conform to an activated phenotype and resemble $CD200^{+/+}$ retinal MG. Both characteristically display ramified forms with no loss of processes. **B:** Three-color flow cytometric assessment of $CD45^{+}CD11b^{+}$ MG show that in both animals there is an equivalent low level of MHC class II, CD40, and CD86 expression (mean fluorescent intensity). The low levels depicted are known to be distinct from background because experiments showed consistent, repeated mean fluorescent intensity levels greater than the limits defined during set up using isotype-positive and -negative controls (mean geometric fluorescent intensity, 2.3 ± 0.9). Original magnifications: ×750 (**Ai**); ×700 (**Aii**).

test, $n = 7$; Figure 1C). Unlike CNS and rat retina,[23] it is not possible in mouse retina to distinguish between MG and perivascular macrophages flow cytometrically because both populations are $CD45^{high}$. Morphologically MG in $CD200^{-/-}$ mice were identical, displaying normal ramified appearance with no loss of processes (Figure 2A). Flow cytometric analysis also demonstrated that these cells expressed equivalent low amounts of CD86 and CD40 and MHC class II as seen in $CD200^{+/+}$ mice (Figure 2B). However, despite these normal morphological features, MG in $CD200^{-/-}$ mice expressed NOS2, normally low or absent in mouse retina (Figure 3).

$CD200^{-/-}$ Mice Demonstrated an Accelerated Severe Onset of IRBP Peptide 1-20-Induced EAU Characterized by Increased $CD11b^{+}$ Infiltration and Retinal Cell Apoptosis

After immunization with IRBP peptide 1-20, both $CD200^{-/-}$ and $CD200^{+/+}$ animals developed EAU with an incidence of 100%. Greatest disease activity was observed day 16 after immunization in $CD200^{-/-}$ mice compared to day 23 in $CD200^{+/+}$ mice (Figure 4A). During peak disease, histology of both groups of animals showed features typical of EAU, including vasculitis, leukocytic infiltrate of the vitreous and retina, formation of retinal folds, and ultimately photoreceptor cell and ganglion cell death (Figure 4, B and C). The accelerated and increased leukocytic infiltration observed in $CD200^{-/-}$ mice was confirmed by both flow cytometry and immunohistochemistry (Figure 4; D to J). Moreover, in later experiments, there was no significant difference in disease scores histologically by day 35 after immunization (data not shown), and no evidence of relapsing disease. Flow cytometric analysis of whole retina showed that $CD200^{-/-}$ retina contained significantly higher numbers of $CD11b^{+}$ cells compared to $CD200^{+/+}$ mice at days 10 ($P < 0.04$) and 23 ($P < 0.03$) (Figure 4D). There was no evidence on morphology or scatter profile during flow cytometry to infer a significant $CD11b^{+}$ granulocyte infiltration, or any significant difference in numbers or distribution of T cell infiltrate in both groups throughout the course of EAU. No proliferation, as determined by detection of Ki67, a nuclear-associated antigen present at all stages of active cell cycle, was detected within retinal cells by flow cytometry (data not shown).

Given the prominence of macrophage infiltration in $CD200^{-/-}$ mice we performed TUNEL staining to determine whether reduced myeloid cell death may explain the increased cell numbers in the tissue during disease. However, we noted that at all time points, apoptosis was significantly increased rather than decreased in $CD200^{-/-}$ mice (Figure 5A), particularly within resident

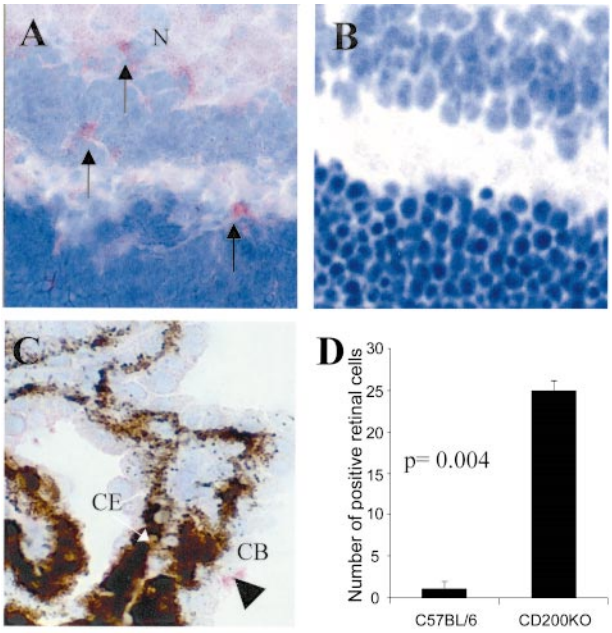

Figure 3. CD200$^{-/-}$ MG display increased constitutive NOS2 expression. Immunohistochemical sections demonstrating NOS2 expression detected with SA:ABC-AP. NOS2-positive MG cells were detected within normal CD200$^{-/-}$ retina (**A**), and primarily absent in CD200$^{+/+}$ retina (**B**). **C** shows that within the CD200$^{+/+}$ eye NOS2 expression was confined primarily to nonretinal sites such as ciliary body (CB) (**arrowhead**; CE, ciliary body epithelium that is pigmented). Counting confirmed that within the retina there is a significant increase in CD200$^{-/-}$ MG NOS2 expression. For quantification, mean NOS2-positive retinal cells were calculated from a minimum of three sections per eye at each time point ($n = 9$; groups of three, three sections per eye). Original magnifications: ×600 (**A**); ×650 (**B**); ×300 (**C**).

cells of the photoreceptor layer and inner nuclear layers of the retina (Figure 5, B and C). This increase was highly significant and was maintained throughout the disease course (day 10, $P < 0.0001$; day 16, $P < 0.0058$; day 23, $P < 0.001$). Dual immunofluorescence confirmed that apoptosis occurred predominantly within non-T cell and macrophage populations (Figure 5, D and E). There was no increase in level of apoptosis in nonimmunized mice (data not shown).

NOS2 expression has been associated with increased apoptosis in inflamed tissue and during EAU, NOS2 expression has been observed before peak disease.[24] Our data now confirms these findings in CD200$^{+/+}$ mice. NOS2 expression in CD200$^{+/+}$ mice peaked at day 16 and was reduced at day 23 coinciding with peak disease scores (Figure 4A). NOS2 expression was significantly higher in CD200$^{-/-}$ mice both before peak disease (day 10, $P < 0.004$) and after peak disease (day 23, $P < 0.035$). However, despite the fact that retinal MG in CD200$^{-/-}$ mice constitutively express higher levels of NOS2 compared to CD200$^{+/+}$ mice, they failed to achieve peak NOS2 expression levels during EAU at the time points tested (Figure 6).

Proliferation Is Unaffected in CD200$^{-/-}$ Mice during EAU

IRBP peptide 1-20 splenocyte proliferative responses were equivalent in both CD200$^{+/+}$ and CD200$^{-/-}$ mice (Figure 7A). This was confirmed, as proliferation was also equivalent in both groups of mice, when T cells and APC were isolated (data not shown). In addition, IFN-γ and IL-10 production in splenocyte culture supernatants stimulated with IRBP peptide 1-20 was measured by ELISA (Figure 7B). IFN-γ was produced to equally high levels in both groups of animals at days 10 and 16 (548 (0.015), 554 (0.002) pg/ml at day 10 and 515 (0.011), 560 (0.06) pg/ml day 16, CD200$^{+/+}$ and CD200$^{-/-}$, respectively) but such a high level was maintained only in CD200$^{-/-}$ mice by day 23 after immunization (162 (0.035) pg/ml *versus* 474 (0.021) pg/ml; $P < 0.0001$, CD200$^{+/+}$ and CD200$^{-/-}$, respectively). IL-10 production was also higher in CD200$^{-/-}$ mice day 23 after immunization (2.9 (0.001) pg/ml *versus* 12.6 (0.008) pg/ml, $P < 0.0001$, CD200$^{+/+}$ and CD200$^{-/-}$, respectively).

Discussion

Macrophage functional development within an inflamed focus must be tightly regulated. It is unknown how that occurs but a classical view from *in vitro* studies suggests it is unlikely to be an aggregated response to all of the stimuli to which they are exposed,[1] and recent data provides evidence that a number of pro- and anti-inflammatory cytokines commit macrophages to develop sets of nonoverlapping and mutually exclusive properties or programs.[8,25,26] Programming is determined by the first cytokine to which macrophages are exposed and an essential component of the program is the development of unresponsiveness to other activating cytokines.[8] Until recently this suggested that the default was that macrophages were uncommitted and therefore susceptible to activation depending on the environment they are exposed to. How this paradigm applies to other related myeloid cell types such as MG is uncertain. The discovery of the CD200 receptor preferentially expressed by myeloid-derived cells together with the widespread distribution of CD200 particularly on endothelium and neural tissue suggested that a cognate receptor-ligand interaction might control the function of macrophages and other myeloid cell types such as MG. This has been supported by observations in experimental autoimmune disease and neurodegeneration models and in CD200$^{-/-}$ mice.[15,16] The current data advances previous findings while supporting the concept of a macrophage regulatory signal after CD200:CD200R engagement. For example, the lack of CD200 results in activation (increased NOS2 expression) and increased numbers of retinal MG. In addition, lack of CD200 results in an accelerated onset of EAU, increased photoreceptor death, and an increased and persistent CD45^{+}CD11b^{+} cell infiltrate throughout disease, representing a predominant macrophage-derived population as no granulocytes were observed morphologically. Despite the difficulty in distinguishing between MG and macrophages in the mouse retina, because the level of CD45 expression is equivalent in both, we observed no Ki-67 expression (nuclear-associated antigen) within MG populations in WT or CD200 knockout mice. Furthermore, during inflammation the

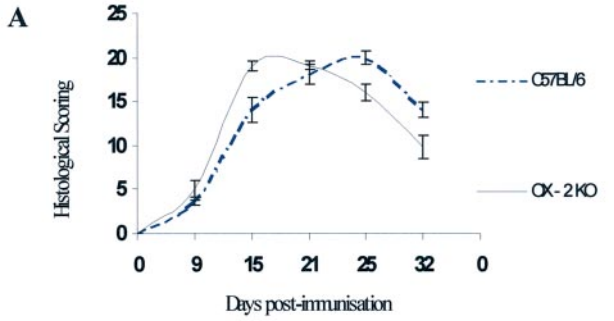

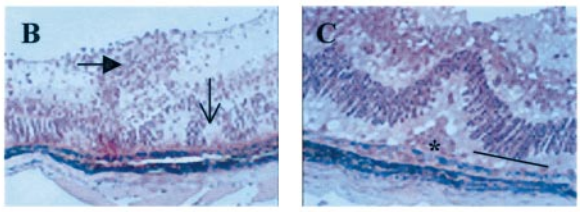

D

		Days Post Immunisation			
		0	10	16	23
Absolute number of $CD45^+CD11b^+$ cells/retina x 10^4 (SD)	$CD200^{+/+}$	2.0(0.13)	7.2(1.4)	39(31)	4.6(1.5)
	$CD200^{-/-}$	2.4(0.29)	12(1.2)	40.4(5.4)	8.9(2.5)
	P Value	0.04	0.04	0.4	0.03

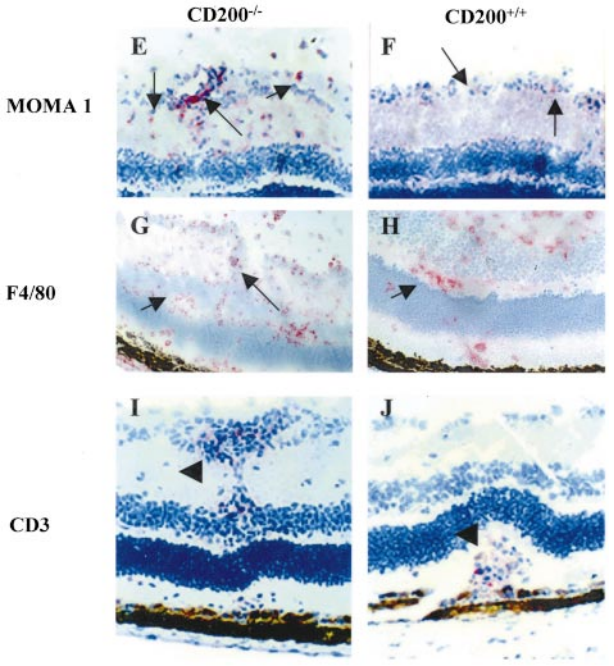

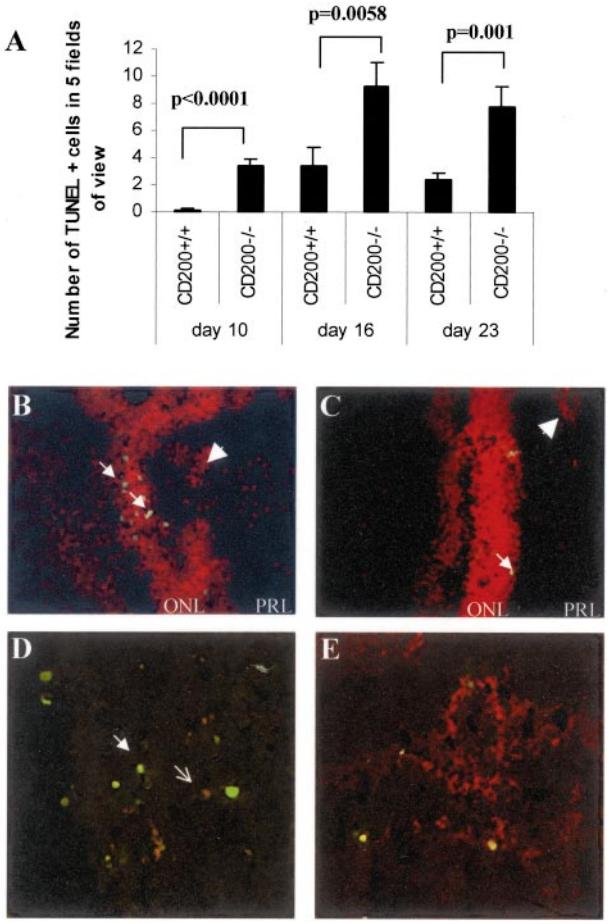

Figure 5. Apoptosis of retinal cells was increased throughout the course of IRBP peptide 1-20 induced EAU. **A:** Histogram shows that there was a significant increase in rate of cellular apoptosis as detected by TUNEL staining in $CD200^{-/-}$ mice. In particular, extent of apoptosis was maintained through the course of disease in $CD200^{-/-}$ mice. Retinal TUNEL-positive cells were counted in five fields of view and mean counts calculated from a minimum of three sections per eye at each time point, $n = 9$. **B** and **C:** TUNEL-positive retinal cells within the outer nuclear layer (ONL) (**arrows**) and not mainly within the foci of infiltrating leukocytes within the photoreceptor layer (PRL) (**arrowheads**) in both $CD200^{-/-}$ and $CD200^{+/+}$, respectively. **D** and **E** demonstrate further that the majority of TUNEL-positive (FITC) cells are not identified as CD3 (**D**, red; **open arrow**) or F4/80 (**E**) dual-stained cells. Original magnifications: ×40 (**A**); ×300 (**B**); ×200 (**C**); ×500 (**D**); ×500 (**E**).

Figure 4. $CD200^{-/-}$ mice have an earlier and increased severity of IRBP peptide 1-20 induced EAU. **A:** Graphic representation of histological scoring of EAU disease severity in $CD200^{-/-}$ and $CD200^{+/+}$mice, graded by combining infiltration levels in anterior and posterior areas with tissue damage. $CD200^{-/-}$ mice have an accelerated onset of disease achieving peak disease earlier than $CD200^{+/+}$mice. Ultimately, the structural damage was not significantly different between the two groups. No difference in clinical disease features between $CD200^{+/+}$ and $CD200^{-/-}$ mice were observed. **B** and **C:** Representative H&E preparations of retinal sections showing EAU features at day 16 after immunization and include retinal folds (**open arrow**), vasculitis (**closed arrow**), and photoreceptor cell destruction (**line**) and granuloma formation (**asterisk**). **D:** Absolute numbers of $CD45^+CD11b^+$ retinal infiltrate during EAU in $CD200^{+/+}$ and $CD200^{-/-}$ mice, confirming earlier and increased inflammation in $CD200^{-/-}$ mice. MOMA-1 (**E** and **F**), F4/80 (**G** and **H**), and CD3 (**I** and **J**) were visualized with SA ABC-AP on section of retinal tissue from $CD200^{-/-}$ mice (**E, G**, and **I**) and $CD200^{+/+}$ mice (**F**, **H**, and **J**). In $CD200^{-/-}$ mice, there is an increased infiltration of MOMA-1 and F4/80 cells (**arrows**) but $CD3^+$ T cell infiltrate (**arrowhead**) is equivalent in both $CD200^{-/-}$ and $CD200^{+/+}$ mice, as confirmed by flow cytometry (**D**). Original magnifications: ×300 (**B**); ×500 (**C**); ×200 (**E**, **F**, **I**, and **J**); ×150 (**G** and **H**).

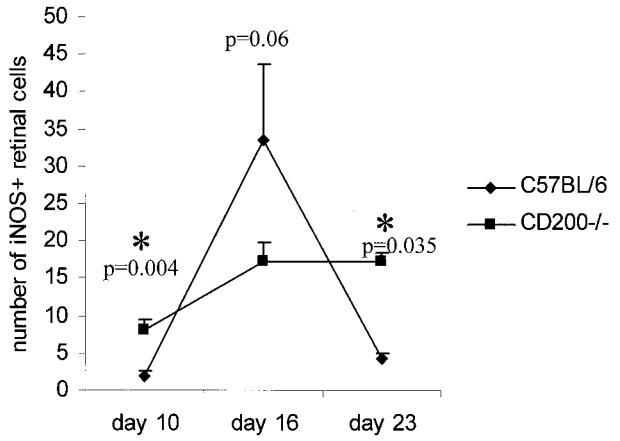

Figure 6. Increased NOS2 expression in CD200$^{-/-}$ at earlier stages of IRBP peptide 1-20 induced EAU but not during peak disease. Line graph representing quantification of NOS2 expression in retinal sections at different phases of EAU. Mean positive NOS2 cells calculated from a minimum of three sections per eye at each time point, $n = 9$.

myeloid cell infiltrate was primarily MOMA-1^{+}F4/80^{+}CD11c^{-}, consistent with myeloid infiltration and not *in situ* proliferation. Even though the data supports CD200 control of macrophage activation, such observations also raise a possibility of CD200 regulation of macrophage trafficking, migration, and survival.[27] CD200 is expressed on endothelium[17,28] and the increase in retinal macrophage infiltrate after depletion of CD200 infers a possible control of macrophage trafficking via CD200:CD200R engagement, and requires further investigation. Despite increased MG numbers within noninflamed normal retina, there was no increase in apoptosis, suggesting that neither the turnover of MG nor resident retinal cell survival is affected by CD200 depletion. However, once inflammation is present there is a significant increase in apoptosis within photoreceptors and inner nuclear cells of the retina.

This study confirms that depletion of CD200 also increases NOS2 expression in macrophages and MG in retina, a specialized neural tissue exhibiting lower numbers of MG than brain. In normal retina, MG are usually NOS2-negative (Figure 3) and significant levels of expression of NOS2 are observed only during peak EAU subsiding again during resolution of inflammation.[24] Correspondingly NOS2 inhibitors protect against photoreceptor destruction[24] and suppress production of peroxynitrite and apoptosis of photoreceptors.[29] MG are conditioned *in situ* and display characteristics of transforming growth factor-β conditioned bone marrow-derived macrophages[8] in that they neither spontaneously nor after stimulation with IFN-γ, produce NO but express β-glucuronidase.[30] It would seem therefore that in the absence of a functional CD200-CD200R axis, macrophages and retinal MG are activated. There was no specific anti-mouse CD200R mAb available, but within the confines of rat retina, where there is abundant expression of CD200, we have previously shown that CD200R was not detected.[17] However, during EAU expression of CD200R is observed readily on both MG and infiltrating CD11b^{+} cells in the rat model.[17] One explanation is that during CD200:CD200R tonic suppression of macrophage activation, MG down-regulate CD200R. It is not clear what the signals are that support up-regulation of CD200R expression in MG during inflammation. Certainly a Th1 response in EAU with pronounced IFN-γ and tumor necrosis factor-α activity[31,32] within the retina, may generate signals, which override the CD200:CD200R axis and activate cells. Given that the data strongly supports that in CD200$^{-/-}$ mice MG are classically activated, we were surprised to observe that firstly; during peak disease, NOS2 expression was reduced compared to CD200$^{+/+}$ mice and to that previously reported,[24,33,34] and secondly there was no significant increase, in photoreceptor destruction observed histologically. One could assume, therefore, that as we have shown CD200$^{-/-}$ mice generate equivalent T cell responses and abundant IFN-γ production, deregulated activated MG and infiltrating macrophages are simply unable to respond further to a classical IFN-γ-mediated increase in NOS2 expression.[8] This may explain why tissue damage, despite our observed earlier disease onset and in-

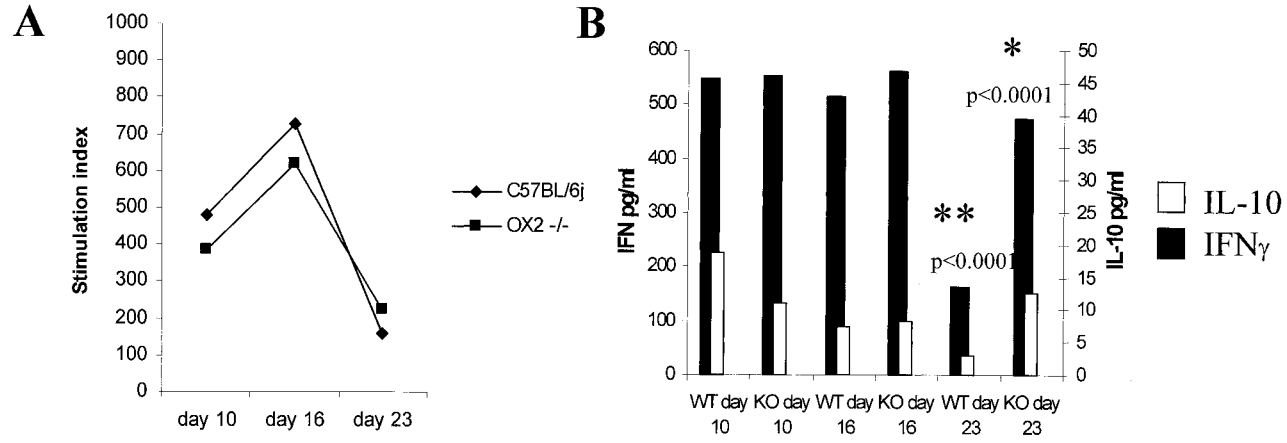

Figure 7. Splenocyte responses are maintained in CD200$^{-/-}$ mice. **A:** Splenocyte responses were equal at each time point between both groups of animals as represented by stimulation indices [background counts were 1120 (109) and Con A responses were 6711(1504) cpm (SD)]. Representative of repeated experiments, supernatants from splenocyte cultures, were further analyzed by capture ELISA for IL-10 and IFN-γ. **B:** There was a significant increase in IFN-γ and IL-10 response in CD200$^{-/-}$ mice 23 days after immunization. Nonstimulated splenocyte supernatants were below detection of ELISA, indicating that the observed response is peptide-specific and not because of the use of adjuvant.

creased levels of macrophage infiltrate, was not enhanced in this model. Although indefinable in this model, the findings of sustained photoreceptor cell apoptosis, together with maintained higher NOS2 expression infer that chronic tissue loss and subsequent functional loss may result in the long term via an inability to recover homeostatic control. Despite increased levels of apoptosis in these current experiments we were unable to observe histologically differences in outer nuclear layer (ONL) cell loss, perhaps because the level of apoptosis precluded ability to observe differences in, for example, total number of cells remaining over rows of cells. We are presently attempting to establish electrophysiological assessment of retinal function to investigate whether our observed ONL apoptosis leads to retinal dysfunction. CD200 depletion alters local tissue control of both resident and myeloid cells, the persistence of cytokine production in $CD200^{-/-}$ (both IFN-γ and IL-10) observed during splenocyte responses also infers a peripheral activation of T cells (although not manifested as an increased proliferation) either directly or indirectly because of altered APC activation, both of which require further investigation.

Concluding Remarks

This data infers that CD200 acts primarily on effector responses that are mediated via interaction with CD200R-expressing macrophages. With respect to retina and CNS, CD200 is an important regulator of myeloid activation *in situ* during inflammation. Constitutive downregulation of CNS and retinal macrophages have important implications on how potential deregulation of CD200: CD200R axis effects not only the course of autoimmune inflammation but also the generation of, and tissue response to, neurodegenerative conditions.

Acknowledgments

We thank Linda Duncan, Neil Taylor, and Morag Robertson for their excellent assistance.

References

1. Forrester JV, McMenamin PG: Immunopathogenic mechanisms in intraocular inflammation. Chem Immunol 1999, 73:159–185
2. Laszlo DJ, Henson PM, Remigio LK, Weinstein L, Sable C, Noble PW, Riches DW: Development of functional diversity in mouse macrophages. Mutual exclusion of 2 phenotypic states. Am J Pathol 1993, 143:587–597
3. Takahashi K, Yamenura F, Naito M: Differentiation, maturation and proliferation of macrophages in yolk sac: a light microscope, enzyme-cytochemical immunohistochemical and ultrastructural study. J Leukoc Biol 1989, 45:87–96
4. Yamada M, Naito M, Takahasi K: Kupffer cell proliferation and glucan induced granuloma formation in mice depleted of blood monocytes by strontium-89. J Leukoc Biol 1990, 47:195–205
5. Rooijen N, Kors N, Vd Endn M, Dijkstra CD: Depletion and repopulation of macrophages in spleen and liver of rat after intravenous treatment with liposome encapsulated di-chloromethylene diphosphate. Cell Tissue Res 1990, 260:215–222
6. Naito M, Umeda S, Yamamoto T, Moriyama H, Umezu H, Hasegawa G, Usuda H, Shultz LD, Takahashi K: Development, differentiation and phenotypic heterogeneity of murine tissue macrophages. J Leukoc Biol 1996, 59:133–138
7. Morioka Y, Naito M, Sato T, Takashi K: Immunophenotypic and ultrastructural heterogeneity of macrophage differentiation in bone marrow and fetal haemopoesis of mouse. J Leukoc Biol 1994, 55:642–651
8. Erwing LP, Kluth DC, Walsh GM, Rees AJ: Initial cytokine exposure determines function of macrophages and renders them unresponsive to other cytokines. J Immunol 1998, 161:1983–1988
9. Lu Q, Lemke G: Homeostatic regulation of the immune system by receptor tyrosinekinases of the Tyro 3 family. Science 2001, 293:306–311
10. Lanier LL, Bakker ABH: The ITAM bearing transmembrane adaptor DAP-12 in lymphoid and myeloid cell function. Immunol Today 2000, 21:611–614
11. Ravetch JV, Lanier LL: Immune inhibitory receptors. Science 2000, 290:84–89
12. Lanier LL: Face-off: the interplay between activating and inhibitory immune receptors. Curr Opin Immunol 2001, 3:326–331
13. Barclay N, Ward H: Purification and chemical characterisation of membrane glycoprotein from rat thymocytes and brain, recognised by monoclonal antibody MRC OX2. Eur J Biochem 1982, 129:447–452
14. Wright G, Puklavec M, Willis AC, Hoek RM, Sedgwick JD, Brown MH, Barclay AN: Lymphoid/neuronal cell surface OX2 glycoprotein recognises a novel receptor on macrophages implicated in the control of their function. Immunity 2000, 13:233–242
15. Hoek R, Ruuls SR, Murphy CA, Wright GJ, Goddard R, Zurawski SM, Blom B, Homola ME, Streit WJ, Brown MH, Barclay AN, Sedgwick JD: Down regulation of the macrophage lineage through interaction with OX2 (CD200). Science 2001, 290:1768–1771
16. Preston S, Wright G, Starr K, Barclay N, Brown M: The leucocyte/neuron cell surface antigen OX2 binds to a ligand on macrophages. Eur J Immunol 1997, 27:1911–1918
17. Dick AD, Broderick C, Forrester JV, Wright GJ: Distribution of OX2 antigen and OX2 receptor within the retina. Invest Ophthalmol Vis Sci 2001, 42:170–176
18. Caspi R, Roberge FG, Chan CC, Wiggert B, Chader GJ, Rozenszajn LA, Lando Z, Nussenblatt RB: A new model of autoimmune disease. Experimental autoimmune uveitis induced in mice with two different retinal antigens. J Immunol 1988, 140:1490–1495
19. Avichezer D, Silver P, Chan CC, Wiggert B, Caspi R: Identification of a new epitope of human IRBP that induces autoimmune uveoretinitis in mice of the H-2b haplotype. Invest Ophthalmol Vis Sci 2000, 41:127–131
20. Dick AD, McMenamin PG, Korner H, Scallon BJ, Ghrayeb J, Forrester JV, Sedgwick JD: Inhibition of TNF activity minimises target organ damage in experimental autoimmune uveoretinitis despite quantitatively normal activated T cell traffik to the retina. Eur J Immunol 1996, 26:1018–1025
21. Adler AJ, Evans CD: Some functional characteristics of purified bovine IRBP. Invest Ophthalmol Vis Sci 1985, 26:273–82
22. Laliotou B, Liversidge J, Forrester JV, Dick AD: IRBP is a potent tolerogen in Lewis rat: suppression of EAU is retinal antigen specific. Br J Ophthalmol 1997, 81:61–67
23. Dick AD, Ford AL, Forrester JV, Sedgwick JD: Cytometric identification of a minority population of MHC class II positive cells in normal rat retina distinct from CD45low CD11b/c+ CD4low parenchymal microglia. Br J Ophthalmol 1995, 79:834–840
24. Hoey S, Grabowski P, Ralston S, Forrester JV, Liversidge J: Nitric oxide accelerates the onset and increases the severity of EAU through an IFNgamma dependent mechanism. J Immunol 1997, 159:5132–5142
25. Lake FR, Noble PM, Henson PM, Riches DWH: Functional switching of macrophage responses to TNFalpha by interferons: implications for the pleiorophic activities of TNFalpha. J Clin Invest 1993, 93:1661–1668
26. Shnyra A, Brewington R, Alipio A, Amura C, Morrison DC: Reprogramming of lipopolysaccharide-primed macrophages is controlled by a counterbalanced production of IL-10 and IL-12. J Immunol 1998, 160:3729–3736
27. Nathan C, Miller WA: Putting the brakes on innate immunity: a regulatory role for CD200? Nature Immunol 2001, 2:17–19

28. Barclay N: Different reticular elements in rat lymphoid tissue identified by localisation of Ia, Thy-1 and MRC OX2 antigens. Immunology 1981, 44:727–736
29. Liversidge J, Dick A, Gordon S: Nitric oxide mediates apoptosis through formation or peroxynitrite and Fas/FasL interactions in experimental autoimmune uveitis. Am J Pathol 2002, 160:905–916
30. Robertson MJ, Erwig LP, Liversidge J, Forrester JV, Rees AJ, Dick AD: Retinal microenvironment controls resident and infiltrating macrophage function during uveoretinitis. Invest Ophthalmol Vis Sci 2002, 43:2250–2257
31. Dick AD, Duncan L, Hale G, Waldmann H, Isaacs J: Neutralising TNF-alpha activity modulates T cell phenotype and function in experimental autoimmune uveoretinitis. J Autoimmunity 1998, 11: 255–264
32. Laliotou B, Dick AD: Modulating phenotype and cytokine production of leucocyte retinal infiltrate in experimental autoimmune uveoretinitis following intranasal tolerance induction with retinal antigens. Br J Ophthalmol 1999, 83:478–485
33. Zhang J, Wu L, Wu G, Rao N: Differential expression of nitric oxide synthase in experimental uveoretinitis. Invest Ophthalmol Vis Sci 1999, 40:1899–1905
34. Wu GS, Zhang J, Rao NA: Peroxynitrite and oxidative damage in experimental autoimmune uveitis. Invest Ophthalmol Vis Sci 1997, 38:1333–1339